Polarized neutron reflectivity and scattering studies of magnetic heterostructures

2003 J. Phys.: Condens. Matter 15 S505

(http://iopscience.iop.org/0953-8984/15/5/306)

INSTITUTE OF PHYSICS PUBLISHING JOURNAL OF PHYSICS: CONDENSED MATTER

J. Phys.: Condens. Matter **15** (2003) S505–S517 PII: S0953-8984(03)55326-7

Polarized neutron reflectivity and scattering studies of magnetic heterostructures

H Zabel and K Theis-Bröhl

Fakultät für Physik und Astronomie, Lehrstuhl für Experimentalphysik/Festkörperphysik, Ruhr-Universität Bochum, D-44780 Bochum, Germany

E-mail: hartmut.zabel@ruhr-uni-bochum.de

Received 29 October 2002
Published 27 January 2003
Online at stacks.iop.org/JPhysCM/15/S505

Abstract

The current interest in the magnetism of ultrathin films and multilayers is driven by their manifold applications in the magneto- and spin-electronic areas, for instance as magnetic field sensors or as information storage devices. In this regard, there is a large interest in exploring spin structures and spin disorder at the interface of magnetic heterostructures, to investigate magnetic domains in thin films and superlattices, and to understand remagnetization processes of various laterally shaped magnetic nanostructures. Traditionally neutron scattering has played a dominant role in the determination of spin structures, phase transitions and magnetic excitations in bulk materials. Today, its potential for the investigation of thin magnetic films has to be redefined. Polarized neutron reflectivity (PNR) at small wavevectors can provide precise information on the magnetic field distribution parallel to the film plane and on layer resolved magnetization vectors. In addition, PNR is not only sensitive to structural interface roughness but also to the magnetic roughness. Furthermore, magnetic hysteresis measurements from polarized small angle Bragg reflections allows us to filter out correlation effects during magnetization reversals of magnetic stripes and islands. An overview is provided on most recent PNR investigations of magnetic heterostructures.

1. Introduction

The area of thin magnetic films and magnetic heterostructures has witnessed impressive progress in recent years. This includes the exchange coupling between similar ferromagnetic layers separated by paramagnetic or semiconducting spacer layers [1] as well as dissimilar layers [2], the exchange bias effect between ferro- and antiferromagnetic layers [3], the exchange spring effect between hard and soft magnetic layers [4], reorientation phase transitions [5] and the proximity effect between ferromagnetic and superconducting layers [6],

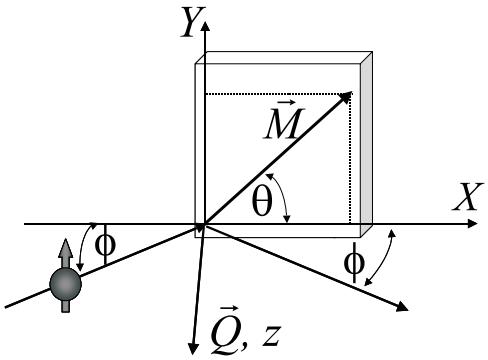

Figure 1. Scattering geometry for PNR studies. The Y axis is the quantization axis for the neutrons and the non-spin-flip axis and the X direction is the spin-flip axis. For specular reflectivity studies the scattering vector $\vec{Q}$ is parallel to the z axis.

just to mention a few of them. Furthermore, the magnetic properties of laterally structured magnetic materials with different shapes and periodicities have created much interest recently [7, 8]. This progress relies, on the one hand, on improved sample preparation techniques for complex material combinations and, on the other hand, on an increasing arsenal of powerful experimental tools for the analysis of their structural and physical properties. Those include SQUID magnetometry, magneto-optical Kerr effect (MOKE), ferromagnetic resonance (FMR) and magnetic force microscopy. More recently, spectroscopic methods, like x-ray circular magnetic dichroism (XCMD), spin resolved photo-emission spectroscopy (SPPS) and polarized electron emission microscopy (PEEM) have been added. Although neutron scattering is best known as a powerful bulk probe, in recent years it has provided invaluable information on exchange coupling [9, 10], on exchange bias [11–14, 16, 17] and on the complex magnetism of ultrathin films [18–20]. Most recently it has been demonstrated that neutron scattering also provides important information on the remagnetization process of patterned magnetic structures [21–23]. In this contribution, a basic introduction to the method of polarized neutron reflectivity (PNR) and scattering is provided, followed by a discussion of selected recent examples, showing that this method plays an essential role for the analysis and understanding of magnetic heterostructures.

2. Remarks on polarized neutron reflectivity

A few basic properties of PNR shall be recalled here for later use. For a more detailed treatment of PNR we refer to [25–29]. Let us assume that a half-infinite sample with a flat surface is in a ferromagnetic, single-domain state. As schematically shown in figure 1, the magnetization vector $\vec{M}$ may lie in the sample plane and perpendicular to the scattering vector $\vec{Q}$. Furthermore, $\vec{M}$ shall make an angel θ against the x axis. Next we assume that a monochromatic and polarized neutron beam is incident onto the sample at a scattering angle ϕ and that the magnetic moment of the incoming monochromatic neutron is aligned normal to the scattering plane and parallel to the sample surface.

With PNR it is possible to measure independently the non-spin-flip (NSF) reflectivities $R^{+,+}$, $R^{-,-}$ and the spin-flip (SF) reflectivities $R^{+,-}$, $R^{-,+}$. From the reflectivities, the nuclear and magnetic potential profile along the sample normal can be retrieved. The difference

$$R^{+,+} - R^{-,-} = 2p_m \sin(\theta) = 2p_Y \propto 2M_Y, \tag{1}$$

is proportional to the Y component of the magnetization vector M_Y, whereas the SF reflectivities

$$R^{+,-} = R^{-,+} \tag{2}$$

are degenerate, and

$$R^{+,-} + R^{-,+} = 2p_m \cos(\theta) \propto M_X^2 \tag{3}$$

is proportional to the square of the X component of the magnetization vector M_X. Here p_m is defined by the magnetic potential which the neutron experiences in the sample:

$$V_m = -\mu \cdot \boldsymbol{B}_{eff,||} = \frac{2\pi\hbar^2}{m} N_A p_m, \tag{4}$$

where μ is the neutron magnetic moment, $\boldsymbol{B}_{eff,||}$ is the effective magnetic induction in the sample plane, m is the neutron mass and N_A is the atomic number density.

The total neutron scattering potential $V_{tot} = V_n + V_m$ consists of a nuclear V_n and a magnetic part V_m and is proportional to the scattering length density of the form

$$N_A b_{eff} = N_A(b \pm p_Y). \tag{5}$$

Here b is the coherent scattering length for neutron nuclear scattering. Accordingly, the critical scattering vector for total external reflection from a non-magnetic sample:

$$Q_{c,z} = \sqrt{16\pi N_A b} \tag{6}$$

is modified for ferromagnetic samples, and for NSF scattering Q_c depends on the sample magnetization and the polarization of the beam:

$$Q_c^{\pm} = \sqrt{16\pi N_A(b \pm p_Y)}. \tag{7}$$

Here $\pm$ refers again to the up and down spin polarization. The SF and NSF reflectivities discussed so far refer to specular PNR, which assumes that the incident angle of the neutron beam to the surface ϕ equals the exit angle. Later we will also discuss off-specular scattering for exploring magnetic roughness and samples with a periodic lateral structure.

3. Experimental considerations

As discussed above, any Y component of a magnetic field distribution or a sample magnetization leads to two critical angles for total neutron reflection with respect to the two possible neutron spin polarizations. If the incident beam is unpolarized, for scattering vectors $\vec{Q}_c^- \leqslant \vec{Q} \leqslant \vec{Q}_c^+$, one polarized beam is reflected and the other one with the opposite polarization is refracted. This property is exploited in supermirrors for polarizing neutron beams, where either the reflected or the transmitted beam is being used for reflectivity measurements [31].

PNR studies are carried out either in a wavelength or in an angle dispersive mode. In the angle dispersive mode a monochromator in the incident beam selects a narrow wavelength band of $\Delta\lambda/\lambda = 0.5$–$5\%$, depending on the resolution required. Instead of a monochromator, a Fermi velocity selector with continuously tunable wavelength and resolution can also be placed in the incident beam. Supermirrors together with π-spin-flip coils (Mezei flippers) are used in the incident and reflected beam for polarizing the beam before the sample and for analysing the polarization state after the scattering event. A typical set-up for an angle dispersive instrument is shown in figure 2. The supermirrors are used in the transmission mode, and in the chosen example the front flipper is turned 'on' to provide a spin-up state, while the back flipper is turned 'off', thus measuring the (+, +) cross section. In figure 3 the angle dispersive ADAM reflectometer at the Institute Laue-Langevin is shown in a cutaway view.

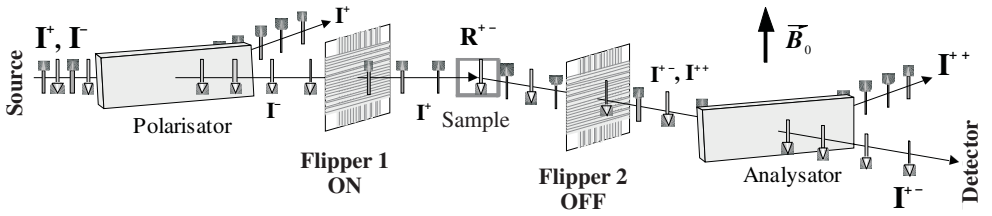

Figure 2. Schematic outline of an angle dispersive neutron reflectometer with polarization analysis. The incident monochromatic and unpolarized beam is polarized by the first supermirror in transmission mode. Spin flippers before and after the sample can change the neutron polarization from up to down and vice versa. The back supermirror analyses the polarization state of the neutrons after the sample. Courtesy Siebrecht [30].

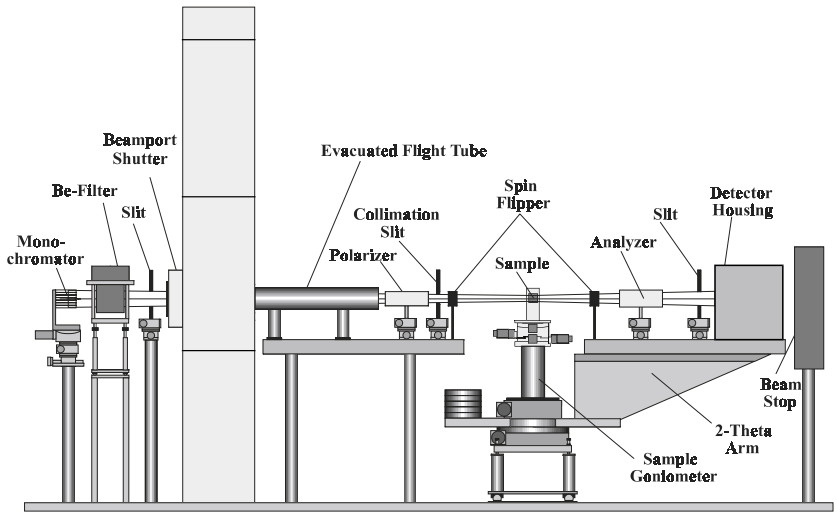

Figure 3. Cutaway view of the angle dispersive neutron reflectometer ADAM at the Institute Laue-Langevin, Grenoble.

Instead of taking radial scans in the $\vec{Q} = Q_z$ direction, i.e. parallel to the specular ridge, it is often necessary to map out the off-specular diffuse intensity by using a position-sensitive detector (PSD). The PSD covers the specular reflection as well as collects off-specular intensity. Such a map is schematically shown in figure 4. The reciprocal space is, in principle, limited by the Yoneda wings, which yield enhanced intensity if either the incident or the scattered beam encloses a critical angle to the surface for total reflection. In this schematic representation of the reciprocal space map it is assumed that a superlattice consists of an antiferromagnetic doubling of the magnetic period as compared to the chemical period. Therefore, the map contains an antiferromagnetic half-order Bragg peak from the doubling of the magnetic period and a full-order Bragg peak from the chemical period. Furthermore, Bragg sheets are shown in the horizontal direction on either side of the specular Bragg peaks. Those sheets are due to correlated roughness. Under the conditions assumed here, the diffuse sheet at the full Bragg peak is due to correlated structural roughness, while the diffuse sheet at the half-order Bragg peak is due to correlated magnetic roughness. The latter may have different causes, being either due to spin disorder at the interfaces or due to a magnetic domain structure which is correlated

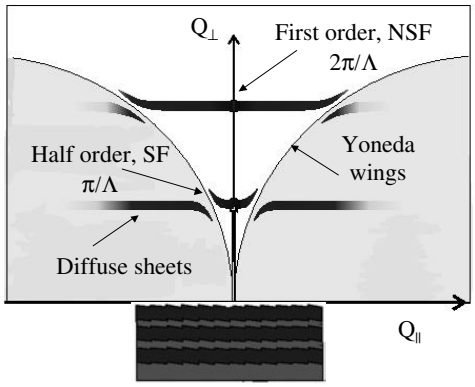

Figure 4. Schematics of a reciprocal space map covering both the specular and the off-specular part. The half-order peak is representative for a doubling of the magnetic periodicity in the case of an antiferromagnetic structure. The full-order peak reflects the chemical periodicity together with any ferromagnetic component. The diffuse scattering occurs in Bragg sheets if the structural or magnetic roughness is correlated from interface to interface.

from one bilayer to the next. The details have to be discussed for each specific case and some of those are mentioned further below. Since most samples are rather transparent for neutrons, scattering beyond the Yoneda wings is possible although the incident or exit neutron beam is then below the horizon of the sample. The advantage of recording a map is the larger reciprocal space area covered in a neutron scan. The disadvantage is the lack of polarization analysis in this configuration. However, simultaneous polarization analysis of the specular and off-specular exit beam is possible by the use of a polarized ^{3}He transmission filter in the exit beam [32]. The technical expenditure is still quite high and the intensity loss is severe. Therefore, using this technique is only recommended if polarization analysis is absolutely necessary.

4. Thin ferromagnetic films

In the following we start our discussion of PNR with measurements from a thin ferromagnetic layer on a non-magnetic substrate. Figure 5 shows polarized reflectivity scans from a single 2 nm thick Fe(110) film on top of a 150 nm thick Nb(110) film grown on a sapphire substrate. The Fe film is protected by a 5 nm thick Nb capping layer. The measurements were carried out at the ADAM instrument of the Institute Laue-Langevin, Grenoble, in an angle dispersive mode [24].

The Fe film is in a ferromagnetic state and the magnetization vector is aligned parallel to the Y axis. Two types of oscillations can be observed. The rapid oscillation is due to the total film thickness including all three layers: the wider oscillation originates from the top Nb protecting layer, while the complete oscillation from the 2 nm thick Fe film is not visible due to the limited scan range. Nevertheless, the special sandwich design provides a very high sensitivity to the ferromagnetic film via magnetic neutron scattering. The oscillations exhibit completely different intensities for the $R^{+,+}$ and $R^{-,-}$ reflectivities, confirming firstly the ferromagnetic state of the sample, and secondly the orientation of the magnetization vector being parallel to the Y axis. The lower panel of figure 5 shows the nuclear and magnetic density profile resulting from a fit to the $R^{+,+}$ and $R^{-,-}$ reflectivities, using the generalized matrix method for describing the polarized reflectivity [28]. As expected, the profiles are only different for the thin ferromagnetic Fe layer. The contrast between Fe and Nb is high for

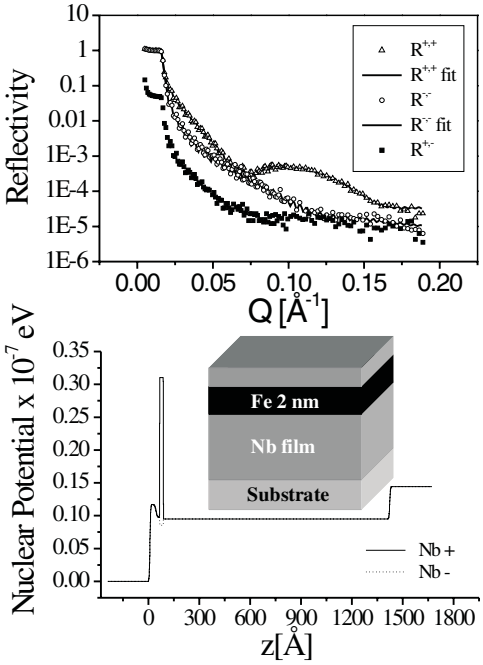

Figure 5. Upper panel: PNRs are shown for a ferromagnetic 2 nm thick Fe layer on a non-magnetic Nb film. The intensity splitting between the $R^{+,+}$ and $R^{-,-}$ reflectivities is a clear sign for the ferromagnetic state of the thin Fe layer. Also shown in the lower part of the figure is the $R^{+,-}$ spin-flip scattering. This scattering is featureless, indicating that any component of the magnetization vector parallel to the X axis is negligible. Lower panel: nuclear and magnetic profile for the up and down neutron spin polarization resulting from a fit to the reflectivity curves according to the generalized matrix method [28].

the neutron polarization parallel to the Fe magnetization vector and low for the antiparallel orientation. The conclusion of this measurement is the very high sensitivity of PNR to thin ferromagnetic layers, corresponding in the present case to only 10^{-3} emu. Obviously this is not the limit and even thinner samples have been investigated in the past [33]. This is an important result, since PNR provides valuable magnetic information on ultrathin buried films together with structural information concerning the film thickness and the magnetization profile. In addition, a quantitative analysis provides absolute magnetic moments, which are free of substrate contributions.

The sensitivity to ultrathin magnetic films can even be enhanced by using a resonator design of the sample, consisting of a ferromagnetic cap layer on a spacer layer, the spacer layer with a scattering length density $N_A b$ (spacer) lower than the combined nuclear and magnetic scattering length density of the ferromagnetic cap layer: $(N_A b + N_A p_Y)$. In this case the reflectivity for $\vec{Q} \leqslant \vec{Q}_c^+$ exhibits pronounced oscillations from the waveguide nature of the spacer layer, leading to an enhanced neutron sensitivity to the magnetic film and interface properties [34].

Another important area of great current interest is thin ferromagnetic films which are exchange coupled to antiferromagnetic layers, resulting in a unidirectional magnetic anisotropy and a shift of the magnetic hysteresis by an exchange bias field H_{EB}, after field cooling the F/AF bilayer below the blocking temperature $T_B \leqslant T_N$ of the AF layer [3]. PNR turns out to be extremely useful for unravelling the magnetic structure of the ferromagnetic film, the domain

structure before and after reversal of the magnetization, and for evaluating the magnetization reversal process itself [11–14]. The technique of a resonator layer mentioned before has recently been exploited for the study of exchange biased CoO/Co films by Radu *et al* [13].

To summarize, the important contribution of PNR to the physics of thin magnetic films is the provision of magnetization profiles and the determination of absolute magnetic moments for ultrathin layers free of diamagnetic contributions. At the same time domain structures and interfacial magnetic roughness is revealed. This information is essential for other methods such as XMCD.

5. Exchange coupling and magnetic roughness in exchange coupled superlattices

Exchange coupled ferromagnetic superlattices have widely been studied in the past because of their unique magnetic and transport properties. Usually the nature of the exchange coupling and coupling strengths are determined from magnetic hysteresis measurements via MOKE or SQUID. Often a non-collinear coupling is encountered in exchange coupled superlattices. In those cases, hysteresis measurements do not properly reveal the angle between the magnetization vectors in adjacent ferromagnetic sheets nor the extent of the magnetic correlation perpendicular to the ferromagnetic sheets. Moreover, often the residual antiferromagnetic coupling is weak and can usually not be distinguished from soft ferromagnetic behaviour. A recent example is the antiferromagnetic coupling of Heusler alloy layers exchange coupled via V spacer layers [15]. The weak antiferromagnetic coupling in the virgin state at low temperatures has only been noticed via PNR. Thus PNR turns out to be essential for revealing coupling angles, in- and out-of-plane correlation lengths, weak antiferromagnetic exchange coupling strength and spin disorder at the interface.

The magnetic roughness has recently been analysed for a Co/Cu multilayer by Borchers *et al* [10], shown in figure 6. The Cu spacer was chosen to be rather thick so as to provide only a weak exchange coupling between the adjacent Co layers. In the as-prepared state of the sample, the Co/Cu multilayer shows a weak half-order antiferromagnetic peak. Polarization analysis confirms strong SF scattering at the half-order position due to antiferromagnetically coupled domains with magnetization vectors perpendicular to the polarization axis. Off-specular scattering clearly shows that the diffuse intensity also peaks at the half-order position. Thus the magnetic diffuse scattering again bunches in Bragg sheets. After applying a magnetic field, the antiferromagnetic coupling is removed and the diffuse scattering is now spread over larger parts of the reciprocal space. Two types of magnetic diffuse scattering can therefore be recognized. One is due to correlated domains, giving rise to the Bragg sheets. The other originates from uncorrelated spins at the interfaces. The two cases are sketched in figure 7. The correlated antiferromagnetic domains yield a diffuse peak in the transverse direction at the half-order position, whose width is inversely proportional to the average lateral domain size. The featureless diffuse scattering is due to uncorrelated magnetic roughness, most likely from spin disorder at the interfaces. A specular component can only be seen when the magnetic domains are larger than the lateral coherence length of the neutron beam. This is usually the case for ferromagnetic peaks in saturation or for antiferromagnetic peaks if the coupling is strong and a uniaxial in-plane anisotropy suppresses domain formation. The magnetic roughness and how it reveals itself in x-ray and neutron scattering experiments is presently of great interest to experimentalists as well as theoreticians. A quantitative analysis of the diffuse magnetic scattering is still under development.

An interesting new approach has recently been described by Lauter-Pasyuk *et al* [35, 36] for the direct determination of the coupling angle of ferromagnetic layers in exchange coupled multilayers. A strong asymmetry in the off-specular neutron SF scattering intensity

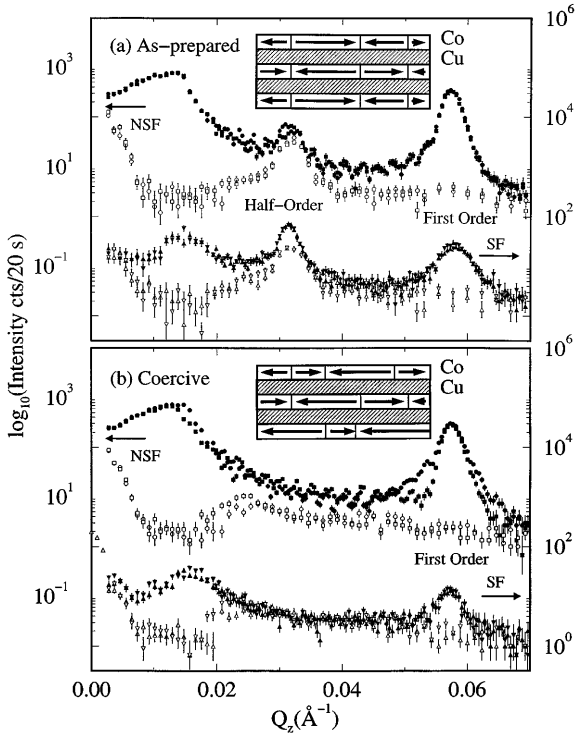

Figure 6. Specular reflectivity scan from a weakly antiferromagnetically coupled Co/Cu multilayer. From [10].

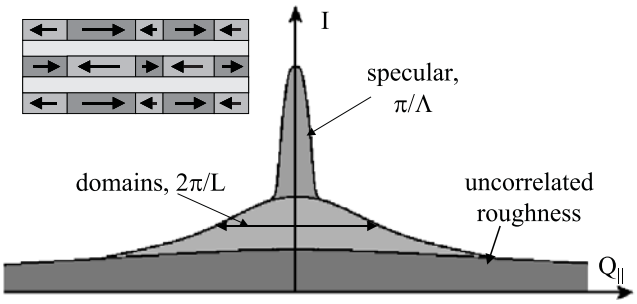

Figure 7. A transverse scan across the half-order Bragg peak is schematically shown together with the different components arising from specular scattering, domain scattering and interfacial roughness.
(This figure is in colour only in the electronic version)

occurs at either the critical incident or the critical exit angle of the half-order SF Bragg sheet, as can be recognized in figure 8. Let us assume that the incident neutron beam is polarized in the (+) state. Then under grazing incidence it will encounter a critical angle ϕ_c of total reflection, characteristic for the nuclear plus magnetic scattering length density: $\phi_c = \arcsin(\lambda\sqrt{n_A(b + p_Y)/\pi})$. Upon spin flip by the sample, the outgoing beam is in a $(-)$ state, for which the critical angle at grazing exit angles is much smaller, or may completely vanish for the case that the difference of the nuclear and magnetic scattering length

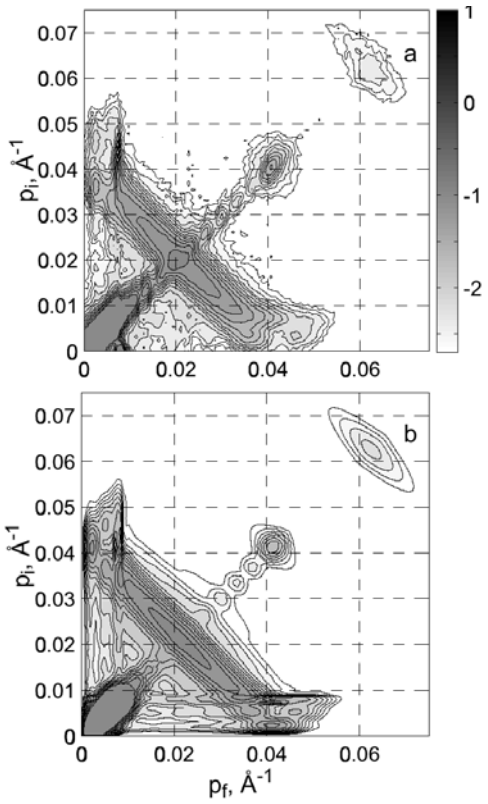

Figure 8. In the upper panel an intensity map is shown on a logarithmic grey scale from a non-collinearly exchange coupled Fe/Cr superlattice, using unpolarized incident neutrons. p_i and p_f refer to the incident and final wave vectors, respectively. The lower panel shows a model fit to the data in the upper panel. The specular as well as the off-specular diffuse scattering at the half-order position can clearly be seen. The off-specular scattering exhibits a characteristic asymmetry, from which the Y component of the magnetic vector can be determined. (Courtesy of Lauter-Pasyuk *et al* [35].)

density becomes negative. For a perfect collinear antiferromagnet in the spin flop state, i.e. all magnetization vectors are aligned parallel to the X axis, the incident beam encounters only a nuclear potential, which does not change upon SF by the magnetization. Then the incident and exit beams are expected to have the same critical angles. However, for a non-collinearly coupled antiferromagnetic structure, the Y component of the magnetization vector adds to the effective potential and is different for the incoming beam as compared to the outgoing SF beam. From ϕ_c the Y component of the layer magnetization can be determined, and thus the coupling angle between the ferromagnetic layers can be reconstructed. An example is shown in figure 8.

To conclude, in the case of multilayers PNR provides indispensable information on even weak antiferromagnetic correlation, on coupling angles and on in- and out-of-plane correlation lengths.

6. Laterally patterned magnetic arrays

Neutron scattering from nanostructured magnetic arrays is a challenging task. Nevertheless it is worth pursuing this task because of the unique information neutron scattering can offer.

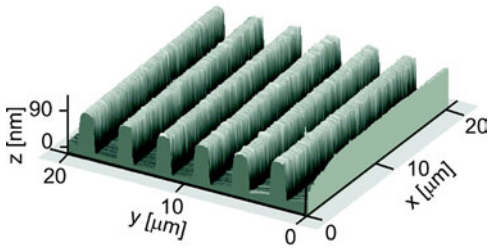

Figure 9. Surface topography of the array of $Co_{0.7}Fe_{0.3}$ stripes obtained with an atomic force microscope shown in a three-dimensional surface view. The displayed area is $20 \times 20\ \mu m^2$.

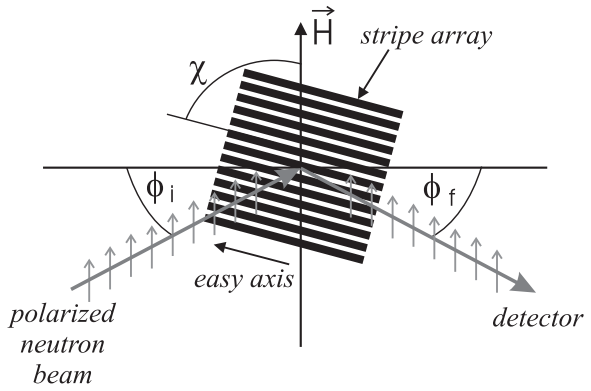

Figure 10. Sketch of the neutron scattering geometry. χ is the angle of the sample rotation with respect to the applied field. The magnetic field $\vec{H}$ is applied perpendicular to the scattering plane. ϕ_i and ϕ_f refer to the incident and exit angles of the neutrons to the sample surface.

However, two experimental difficulties have to be overcome to successfully use this method for laterally structured arrays: first a large and homogeneously structured sample area is required, and second, unfavourable scattering vectors often need to be probed from arrays patterned on a micro- and submicrometre scale.

In the following we show an example for the analysis of the magnetization reversal of a stripe pattern (see figure 9) with neutron scattering. The scattering geometry for the investigation of magnetic stripes is depicted in figure 10. Due to the high aspect ratio, the easy axis in this pattern is aligned parallel to the stripes and in remanence the stripes are in a single domain state. The easy axis corresponds to $\chi = 0°$ and the hard axis to $\chi = 90°$.

Magnetization reversal measurements have been carried out using polarized neutron scattering at small angles [23]. In particular, the first-order Bragg peak of the stripe pattern was scanned for different sample rotation angles χ and the magnetic contribution to the Bragg peak was determined from a spin asymmetry related expression of the polarized intensities according to

$$S'_a = \frac{\sqrt{I_{+,+} + I_{+,-}} - \sqrt{I_{-,-} - I_{-,+}}}{\sqrt{I_{+,+} + I_{+,-}} + \sqrt{I_{-,-} + I_{-,+}}}, \tag{8}$$

with S'_a being proportional to the magnetization component along the y axis:

$$S'_a \propto M_Y.$$

By assuming equivalent spin-flip cross sections $(+,-)$ and $(-,+)$, from the $I(H)$ intensity

values of the three cross sections (+, +), (−, −) and (+, −) a magnetization curve can be calculated, which is proportional to the field-dependent magnetization of the stripes.

The left column of figure 11 shows hysteresis measurements performed at the first-order Bragg peak via polarized neutron scattering. The top row in figure 11 for $\chi = 0°$ exhibits a large splitting of the (+, +) and (−, −) intensities, which reverses suddenly at the coercive field H_c. There is almost no spin-flip scattering visible over the entire field range, indicating that the magnetization reversal for the easy axis configuration takes place in the form of nucleation and fast domain wall movements at H_c. At $\chi = 45°$ the (+, +) − (−, −) splitting starts to become reduced for field values far above and below H_c, while the spin-flip scattering shows a gentle slope towards the coercive field. This behaviour indicates a coherent rotation of the magnetization vector into the field direction. The situation is more pronounced for the sample rotation of $\chi = 63°$. The (−, −) intensity continuously decreases with increasing field from negative to positive field values, while the (+, +) intensity is more or less constant for most of the field values and changes suddenly at the coercive field. At the same time the spin-flip intensity increases again towards the coercive field, however with a larger slope. All four cross sections are again consistent with a coherent rotation of the magnetization vector away from the easy axis.

More quantitative statements can be made by evaluating S'_a, using the $I(H)$ intensities of the four cross sections (+, +), (−, −), (+, −). The neutron hysteresis curves (open squares) are compared to the respective longitudinal MOKE hysteresis loops (full and dotted curves) for the same sample rotation, as shown in the bottom graphs of figure 11. The overall agreement is rather good for all three sample rotation angles. Small deviations are only visible for $\chi = 63°$ close to the coercive field.

The neutron scattering results confirm that, for most of the field values, the stripes are in a single domain state. In the case that the field is applied parallel to the stripe axis (easy axis), a domain nucleation and domain wall movement occurs within a narrow field range at the coercive field. For all other sample orientations a coherent magnetization rotation with increasing field is observed with some domain nucleation occurring just around H_c. However, for a stripe orientation perpendicular to the applied field the domain rotation is complete without nucleation processes. Similar experiments on magnetic dots and magnetic bars have been carried out by Temst *et al* [21, 22].

So far neutron experiments on laterally structured films have concentrated on domain rotation. However, neutron scattering can also provide information on the nucleation process. Combining results from the SF and the NSF cross sections allows us to derive values for the angle and the length of the magnetization vector $\vec{M}$. A constant length of the magnetization vector accounts for rotational processes and a changing length for domain nucleation and domain wall movement. The real power of neutron scattering is, however, only exploited when more complex structures are investigated with interaction between different structural units. Then fluctuations and correlation effects can be worked out.

7. Summary and conclusions

The analysis and understanding of new magneto-electronic heterostructures is an important field with much potential for PNR investigations. Only a few examples could be discussed here. Not mentioned have been exchange coupled double superlattices with interfacial exchange bias effect [17], spring magnets composed of soft and hard magnetic layers [37] and magnetic semiconductor superlattices [38]. For the performance of spin-electronic devices it is presently not clear whether disorder of local moments or the magnetic field distribution is the more important parameter. It must also be tested to what extent spin flip of neutrons yields information on the spin flip of electrons in these magnetic heterostructures.

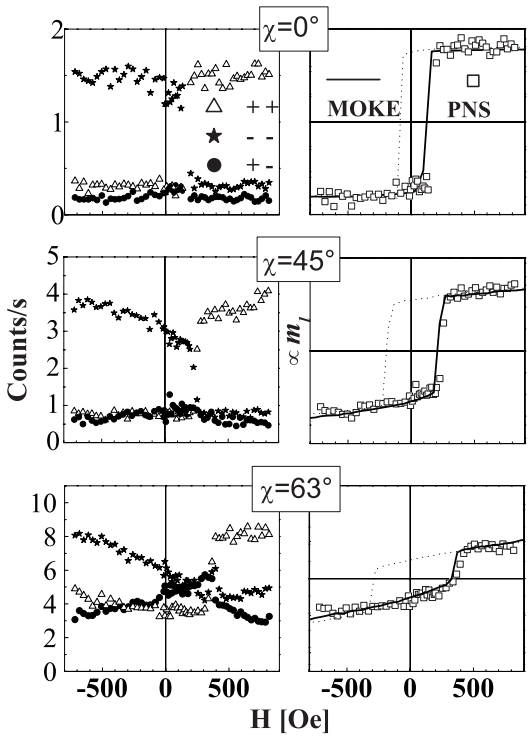

Figure 11. Magnetization reversal measurements performed at the first-order Bragg peak for three different cross sections (left column) and calculated curves from the polarized neutron measurements (right column). The calculated curves are compared to longitudinal MOKE hysteresis loops, reproduced as full and dotted curves. The top row depicts measurements at a sample rotation of $\chi = 0°$, the middle row shows measurements at a sample rotation of $\chi = 45°$ and the bottom row shows measurements at a sample rotation of $\chi = 63°$. From [23].

The benefits of PNR and scattering for the investigation of magnetic nano- and heterostructures can be summarized as:

- direct probe of atomic moments and magnetic induction;
- cross section is known accurately;
- both ferromagnetic and antiferromagnetic structures can be studied easily;
- sensitivity to spin disorder and spin fluctuations;
- magnetic correlation lengths can be probed on different length scales.

Acknowledgments

The authors would like to acknowledge fruitful discussions with Boris Toperverg and Florin Radu, who also provided the scattering profile in figure 5. This work was supported by DFG, SFB 491 and by the BMBF under contract O3ZAE8BO.

References

[1] Bürgler D E, Grünberg P, Demokritov S O and Johnson M T 2001 Interlayer exchange coupling in layered magnetic structures *Handbook of Magnetic Materials* vol 13, ed K H J Buschow (Amsterdam: Elsevier) p 1

[2] Bovensiepen U, Wilhelm F, Srivastava P, Poulopoulos P, Farle M, Ney A and Baberschke K 1998 *Phys. Rev. Lett.* **81** 2368

[3] Nogués J and Schuller I K 1999 *J. Magn. Magn. Mater.* **200** 552
[4] Haskel D, Srajer G, Lang J C, Pollmann J, Nelson C S, Jiang J S and Bader S D 2001 *Phys. Rev. Lett.* **87** 207201
[5] Baberschke K 1996 *Appl. Phys.* A **62** 417
[6] Garifullin I A 2002 *J. Magn. Magn. Mater.* **240** 571
[7] Aign T, Meyer P, Lemerle S, Jamet J P, Ferre J, Mathet V, Chappert C, Gierak J, Vieu C, Rousseaux F, Launois H and Bernas H 1998 *Phys. Rev. Lett.* **81** 5656
[8] Yu J, Rüdiger U, Kent A B, Thomas L and Parkin S S P 1999 *Phys. Rev.* B **60** 7352
[9] Schreyer A, Majkrzak C F, Zeidler T, Schmitte T, Bödeker P, Theis-Bröhl K, Abromeit A, Dura J and Watanabe T 1997 *Phys. Rev. Lett.* **79** 4914
[10] Borchers J A, Dura J A, Unguris J, Tulchinsky D, Kelley M H, Majkrzak C F, Hsu S Y, Loloee R, Pratt W P and Bass J 1999 *Phys. Rev. Lett.* **82** 2796
[11] Fitzsimmons M R, Yashar P, Leighton C, Schuller I K, Nogues J, Majkrzak C F and Dura J A 2000 *Phys. Rev. Lett.* **84** 3986
[12] Leighton C, Fitzsimmons M R, Hoffmann A, Dura J, Majkrzak C F, Lund M S and Schuller I K 2002 *Phys. Rev.* B **65** 064403
[13] Radu F, Etzkorn M, Schmitte T, Siebrecht R, Schreyer A, Westerholt K and Zabel H 2002 *J. Magn. Magn. Mater.* **240** 251
[14] Gierlings M, Prandolini M J, Fritzsche H, Gruyters M and Riegel D 2002 *Phys. Rev.* B **65** 092407
[15] Westerholt K, Bergmann A, Leiner V and Zabel H, to be submitted
[16] te Velthuis S G E, Berger A, Felcher G P, Hill B K and Dan Dahlberg E 2000 *J. Appl. Phys.* **87** 5046
[17] te Velthuis S G E, Felcher G P, Jiang S, Inomata A, Nelson C S, Berger A and Bader S D 1999 *Appl. Phys. Lett.* **75** 4174
[18] Fullerton E E, Bader S D and Robertson J L 1996 *Phys. Rev. Lett.* **77** 1382
[19] Bödeker P, Schreyer A and Zabel H 1999 *Phys. Rev.* B **59** 9408
[20] Leiner V, Labergerie D, Siebrecht R, Sutter Ch and Zabel H 2000 *Physica* B **283** 167
[21] Temst K, Van-Bael M J and Fritzsche H 2001 *Appl. Phys. Lett.* **79** 991
[22] Temst K, Van-Bael M J, Moshchalkov V V, Bruynseraede Y, Fritzsche H and Jonckheere R 2002 *Appl. Phys.* A **74** 51538
[23] Theis-Bröhl K, Schmitte T, Leiner V, Zabel H, Rott K, Brückl H and McCord J 2002 *Phys. Rev.* B submitted
[24] Schreyer A, Siebrecht R, Englisch U, Pietsch U and Zabel H 1998 *Physica* B **248** 349
[25] Felcher G P *et al* 1987 *Rev. Sci. Instrum.* **58** 609
[26] Majkrzak C F 1989 *Physica* B **156/157** 619
[27] Blundell S J and Bland J A C 1992 *Phys. Rev.* B **46** 3391
[28] Radu F and Ignatovich V K 1999 *Physica* B **267/268** 175
[29] Fermon C, Ott F and Menelle A 1999 *X-Ray and Neutron Reflectivity: Principles and Applications (Springer Lecture Notes in Physics)* ed J Daillant and A Gibaud (Berlin: Springer) p 163
[30] Siebrecht R 2001 *PhD Thesis* Ruhr-Universität Bochum
[31] Krist T, Pappas C, Keller T and Mezei F 1995 *Physica* B **213** 939
[32] Nickel B, Rühm A, Donner W, Major J, Dosch H, Schreyer A, Zabel H and Humblot H 2001 *Nucl. Phys. Instrum.* **72** 163
[33] Blundell S J, Gester M, Bland J A C, Lauter H J, Pasyuk V V and Petrenko A V 1995 *Phys. Rev.* B **51** 9395
[34] Aksenov V L, Nikitenko Y V, Radu F, Gledenov Y M and Sedyshev P V 2000 *Physica* B **276** 946
[35] Lauter-Pasyuk V, Lauter H J, Toperverg B, Kravtsov E, Ustinov V, Romashev L and Nikonov O 2001 *J. Magn. Magn. Mater.* **226–230** 1694
[36] Lauter-Pasyuk V, Lauter H J, Toperverg B, Romashev L and Ustinov V 2002 *Phys. Rev. Lett.* **89** 167203
[37] O Donovan K V, Borchers J A, Majkrzak C F, Hellwig O and Fullerton E E 2002 *Phys. Rev. Lett.* **88** 067201
[38] Kępa H, Kutner-Pielaszek J, Twardowski A, Majkrzak C F, Sadowski J, Story T and Giebultowicz T M 2001 *Phys. Rev.* B **64** 121302(R)